JACS
JOURNAL OF THE AMERICAN CHEMICAL SOCIETY
Article
pubs.acs.org/JACS

Development of a Mitochondria-Targeted Hsp90 Inhibitor Based on the Crystal Structures of Human TRAP1

Changwook Lee,*[,†,#] Hye-Kyung Park,[†,#] Hanbin Jeong,[†] Jaehwa Lim,[†] An-Jung Lee,[†] Keun Young Cheon,[†] Chul-Su Kim,[‡] Ajesh P. Thomas,[§] Boram Bae,[§] Nam Doo Kim,[∥] Seong Heon Kim,[∥] Pann-Ghill Suh,[†] Ja-Hyoung Ryu,*[,§] and Byoung Heon Kang*[,†]

[†]Department of Biological Sciences, [‡]UNIST Central Research Facility, and [§]Department of Chemistry, Ulsan National Institutes of Science and Technology (UNIST), Ulsan, 689-798, Korea

[∥]New Drug Development Center, Daegu-Gyeongbuk Medical Innovation Foundation, Daegu, 701-310, Korea

Supporting Information

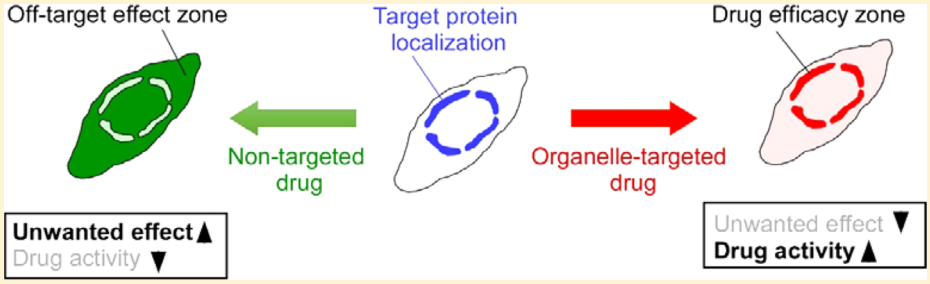

ABSTRACT: The mitochondrial pool of Hsp90 and its mitochondrial paralogue, TRAP1, suppresses cell death and reprograms energy metabolism in cancer cells; therefore, Hsp90 and TRAP1 have been suggested as target proteins for anticancer drug development. Here, we report that the actual target protein in cancer cell mitochondria is TRAP1, and current Hsp90 inhibitors cannot effectively inactivate TRAP1 because of their insufficient accumulation in the mitochondria. To develop mitochondrial TRAP1 inhibitors, we determined the crystal structures of human TRAP1 complexed with Hsp90 inhibitors. The isopropyl amine of the Hsp90 inhibitor PU-H71 was replaced with the mitochondria-targeting moiety triphenylphosphonium to produce SMTIN-P01. SMTIN-P01 showed a different mode of action from the nontargeted PU-H71, as well as much improved cytotoxicity to cancer cells. In addition, we determined the structure of a TRAP1−adenylyl-imidodiphosphate (AMP-PNP) complex. On the basis of comparative analysis of TRAP1 structures, we propose a molecular mechanism of ATP hydrolysis that is crucial for chaperone function.

INTRODUCTION

Expression and activity of Hsp90 are elevated in most cancer cells, where the Hsp90 plays important roles in the survival of malignant cells, which are often exposed to stress conditions.[1] Because of the dependence of cancer cells on the prosurvival functions of Hsp90, many chemical inhibitors targeting the chaperone as anticancer agents have been developed to date, and some are already in clinical trials.[2,3] However, in contrast to early hopes, the activity of inhibitors as single agents was modest;[4] therefore, current clinical trials of Hsp90 inhibitors are mainly focused on combinations with other cancer drugs.[2]

In addition to Hsp90 in the cytoplasm, the mitochondrial pool of Hsp90 and its mitochondrial paralogue, TNF receptor-associated protein 1 (TRAP1), has been found to be elevated in cancer cells,[5,6] where these proteins suppress cell death and reorganize cellular metabolic pathways to promote tumorigenesis.[5,7−11] Therefore, TRAP1 and mitochondrial Hsp90 have been proposed as target proteins for cancer drug development.[12,13] In this regard, mitochondria-targeted Hsp90 inhibitors, the gamitrinibs, which are conjugates of an ansamycin Hsp90 inhibitor (geldanamycin) and a mitochondria-targeting moiety (cyclic guanidinium or triphenylphosphonium), have been developed.[14−17] Gamitrinibs showed strong anticancer activity not only in *in vitro* cell-based assays, but also in *in vivo* preclinical studies,[18−20] and can sensitize cancer cells to additional cellular stresses.[18,21,22]

Although the presence of both Hsp90 and TRAP1 in the mitochondria, with overlapping functions, has been reported before,[5] the relative amounts of the proteins have never been compared. Consistent with this, development of TRAP1-specific inhibitors has not been actively explored due, in part, to the lack of structural information. Here, we argue that TRAP1, rather than Hsp90, is the major chaperone in cancer cell mitochondria and report, for the first time, the crystal structures of human TRAP1 complexed with the purine-scaffold Hsp90 inhibitors PU-H71 and BIIB-021 and the ATP analogue adenylyl-imidodiphosphate (AMP-PNP). On the basis of the structure

Received: November 21, 2014
Published: March 18, 2015

DOI: 10.1021/ja511893n
J. Am. Chem. Soc. 2015, 137, 4358−4367

of the TRAP1−PU-H71 complex, we rationally designed conjugates of Hsp90 inhibitors with a mitochondria-targeting moiety, triphenylphosphonium (TPP), to selectively inactivate mitochondrial TRAP1.

MATERIALS AND METHODS

Chemicals and Antibodies. MitoTracker and tetramethylrhodamine methyl ester (TMRM) were purchased from Molecular Probes. All other chemicals were purchased from Sigma. Antibodies used in this study were anti-CHOP, anti-Hsp90, anti-Hsp70, anti-TRAP1, and anti-COX-IV from BD Biosciences; anti-phospho-eIF2α, anti-eIF2α, anticytochrome *c*, anti-Chk1, and anti-Akt from Santa Cruz Biotechnology; and anti-β-actin from MP Biomedicals.

Cells and Cell Culture. Human cancer cells originating from ovary (SK-OV3), prostate (22Rv1 and PC3), cervix (HeLa), breast (MDA-MB-231), liver (SK-HEP-1), brain (A172), kidney (ACHN), and lung (NCI-H460) were purchased from the Korean Cell Line Bank. Cells were cultured in DMEM or RPMI (Life Technologies) containing 10% fetal bovine serum (FBS; Life Technologies) and 1% penicillin/streptomycin (Life Technologies) at 37 °C in a humidified atmosphere of 10% CO_2. Primary hepatocytes were isolated from 8-week-old BALB/c mice as described previously.[23] Briefly, mice were anesthetized, and the livers were perfused with collagenase solution, dissected, disrupted by pipetting of clumps, and filtered through a 100-μm cell strainer (BD Biosciences). Cells were washed several times by repeated centrifugation and resuspension in M199/EBSS medium (Hyclone). Cell debris and nonparenchymal cells were separated from hepatocytes by gradient centrifugation with Percoll (Sigma). After repeated washing, cell pellets were resuspended and incubated in M199/EBSS medium containing 10% FBS at 37 °C in an atmosphere of 5% CO_2.

Protein Production. The expression and purification of TRAP1 were carried out as described previously.[24] Briefly, human TRAP1 comprising residues 60−561, designated as hTRAP1-NM, with an N-terminal hexahistidine (His_6) tag was expressed in *Escherichia coli* BL21(DE3) cells cultured at 20 °C in the presence of 0.4 mM IPTG. Cells were harvested 15 h postinduction and lysed by sonication, and the protein was purified by Ni^{2+}-IMAC chromatography. The His_6 tag was removed using TEV protease (Invitrogen), and the protein was purified further by ion exchange (HiTrap Q column, GE Healthcare) and size-exclusion (Superdex 200 column, GE Healthcare) chromatography. Selenomethionine-substituted protein was prepared by expressing the recombinant hTRAP1-NM in *E. coli* B834(DE3) cells (Novagen) cultured in M9 minimal media supplemented with selenomethionine. Proteins were concentrated to 20 mg/mL and flash-frozen in liquid nitrogen for storage.

Crystallization and Structure Determination of Human TRAP1-Inhibitor Complexes. Prior to crystallization experiments, hTRAP1-NM was mixed with inhibitors (PU-H71, BIIB-021, SMTIN-P01) in a 1:2 molar ratio and incubated for 30 min on ice. Each complex was crystallized at 22 °C by the hanging-drop method by adding 1 μL of a 9 mg/mL protein solution to 1 μL of well solution comprising 16% PEG 8K, 100 mM calcium acetate, and 100 mM sodium cacodylate, pH 6.5. The crystals are tetragonal, space group $P4_12_12$ ($a = b = 69.5$ Å, $c = 252.5$ Å), and contain one molecule in the asymmetric unit. For X-ray diffraction experiments, crystals were transferred to a well solution containing 30% glycerol and then flash-frozen in liquid nitrogen. Single-wavelength anomalous diffraction (SAD) data were collected with a SeMet crystal of the hTRAP1-NM−PU-H71 complex at beamline 5C of the Pohang Accelerator Laboratory (PAL) and processed using HKL-2000 software.[25] Native data for the hTRAP1-NM−PU-H71, hTRAP1-NM−BIIB-021, and hTRAP1-NM−SMTIN-P01 complexes were collected from single frozen crystals at the same PAL beamline and were integrated and scaled as before. The SAD data analysis was performed using Phenix software[26] and data between 50 and 2.9 Å resolution. Phenix found 10 of the 11 selenium sites and refined these to give a mean figure-of-merit (FOM) of 0.472. Electron density modification using RESOLVE software[27] yielded an initial electron density map of excellent quality. The electron density maps for the hTRAP1-NM−BIIB-021 and hTRAP1-NM−SMTIN-P01 complexes were calculated using hTRAP1-NM−PU-H71 as a model and difference Fourier analysis. Final refinement of the models used the program Phenix.[26] The final model contains one TRAP1 inhibitor for each complex in the asymmetric unit. Of these, the following residues were not modeled due to weak electron densities: TRAP1 residues 60 to 68, 172 to 201, 351 to 361, 398 to 407, and 553 to 561 in the hTRAP1-NM−PU-H71 and hTRAP1-NM−SMTIN-P01 complexes; and residues 60 to 68, 171 to 201, 351 to 361, 398 to 407, 493 to 494, and 553 to 561 in the hTRAP1-NM−BIIB-021 complex. The refinement statistics and composition of the final models are summarized in Supporting Information, Table S1.

Crystallization and Structure Determination of Human TRAP1−AMP-PNP Complex. For the hTRAP1-NM−AMP-PNP complex, a protein solution (1 μL) was mixed with an equal volume of 23% PEG 4K, 100 mM Tris, and 0.35 M ammonium sulfate, pH 8.5. Crystals (space group $P6_5$; $a = b = 115.5$ Å, $c = 339.9$ Å) grew in 2 weeks at 4 °C. For diffraction experiments, crystals were transferred to a well solution containing an additional 30% glycerol and flash-frozen in liquid nitrogen. X-ray diffraction data were collected at the same PAL beamline and processed as above. The structure was solved by molecular replacement with the program Phaser[28] using hTRAP1-NM−PU-H71 as the search model. An initial model of TRAP1 was improved by rigid-body and positional refinement, and the hTRAP1-NM−AMP-PNP structure was built in the resulting electron density map. Final refinement yielded an *R*-factor of 22.0% (R_{free} = 28.5%) for data between 50 and 3.3 Å resolution (Supporting Information, Table S1). The final model consists of 14245 protein atoms and contains four copies of hTRAP1-NM−AMP-PNP in the asymmetric unit. Of these, the following residues were not modeled due to weak electron densities: TRAP1 residues 60 to 69, 188 to 190, 302 to 309, 353 to 361, and 455 to 561 in the first copy; residues 60 to 69, 187 to 190, 354 to 361, and 554 to 561 in the second copy; residues 60 to 69, 188 to 189, 352 to 361, and 554 to 561 in the third copy; and residues 60 to 69, 187 to 191, 358 to 360, 491 to 493, 504 to 523, and 551 to 561 in the fourth copy. The X-ray data and refinement statistics are summarized in Supporting Information, Table S1.

Analysis of Cell Viability. Cells (5×10^3 cells/well) were cultured in 96-well plates overnight and treated with drugs for 24 h. To determine cell viability, cells were exposed to 3(4,5-dimethyl-thyzoyl-2-yl)2,5 diphenyltetrazolium bromide (MTT), and crystallized formazan was quantified by measuring the absorbance at 595 nm with an Infinity M200 microplate reader (Tecan). Absorbance data were compared with those of cells treated with vehicle control and expressed as percent viability.

ATPase Activity Assay. ATPase activity was measured with the PiColorLock Gold Phosphate Detection Kit (Innova Biosciences) by determining release of inorganic phosphate according to the manufacturer's instructions. Either Hsp90 or TRAP1 (0.2 μM) was incubated with 0.2 mM ATP in 100 mM Tris, 20 mM KCl, and 6 mM $MgCl_2$, pH 7.0, for 3 h at 37 °C. Then, the 20 μL mixture of P_iColorLock Gold reagent and the accelerator (100:1) was added to the 80 μL ATP hydrolysate sample. After 5 min incubation at 25 °C, color development was stopped by the addition of 10 μL stop solution, and absorbance was measured at 620 nm with an Infinity M200 microplate reader (Tecan). K_m and k_{cat} values were measured by assaying the activity using 50−1000 μM ATP. For inhibition analysis, Hsp90 and TRAP1 were preincubated with indicated concentration (0.1−30 μM) of inhibitors for 30 min at 37 °C before mixing with ATP.

Analysis of Drug Accumulation in Mitochondria. Mouse brain mitochondria were isolated as previously described.[5] Mitochondria (100 μg) were incubated with 10 μM gamitrinib, PU-H71, DMAG, BIIB-021, or AUY922 for 30 min at 30 °C in mitochondrial incubation buffer (MIB; 0.2 M sucrose, 10 mM Tris-MOPS, pH 7.4, 5 mM succinate, 1 mM Pi, 2 μM rotenone, and 10 μM EGTA). The mitochondria were chilled on ice and collected by centrifugation at 8000*g* for 10 min. The supernatant was collected and the mitochondrial pellet was washed twice with ice-cold MIB and dissolved in lysis buffer (acetonitrile/methanol, 3:1). The concentration of the drug in supernatant and mitochondrial extract was analyzed using a UPLC/Xevo TQ-S mass spectrometer (Waters).

DOI: 10.1021/ja511893n
J. Am. Chem. Soc. 2015, 137, 4358−4367

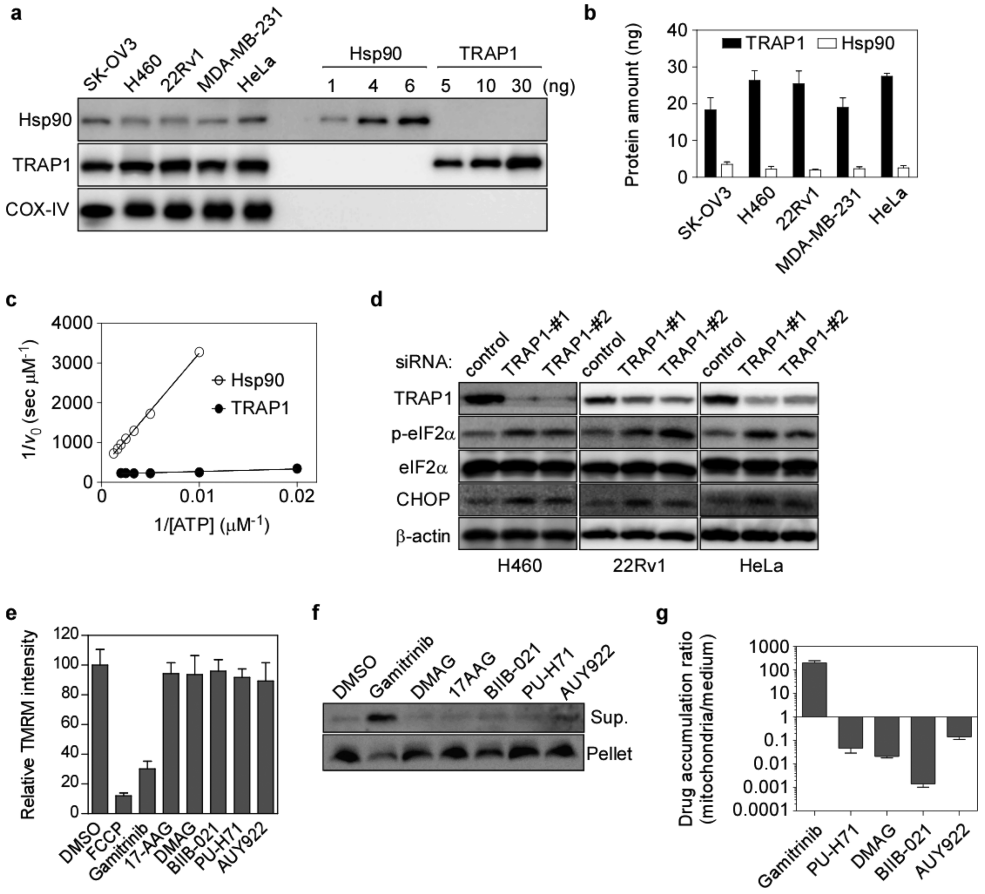

Figure 1. TRAP1, rather than Hsp90, is the predominant chaperone in cancer cell mitochondria. (a,b) Western analysis of Hsp90 and TRAP1 in mitochondria isolated by fractionation of cancer cells from human ovary (SK-OV3), lung (H460), prostate (22Rv1), breast (MDA-MB-231), and cervix (HeLa) (a) and quantitation based on densitometric analysis of the blot (b). Data are mean ± SEM of three independent experiments. COX-IV served as an internal control. (c) ATPase activity of Hsp90 and TRAP1. The initial rate of ATP hydrolysis (v_0) is depicted in the double-reciprocal plot. Data are mean ± SEM of duplicate samples from two independent experiments. (d) Western analysis of ER stress response (elevation of C/EBP homologous protein [CHOP]) and increased phosphorylation of eukaryotic translation initiation factor [eIF]2α) in the indicated cell types after siRNA-mediated TRAP1 knockdown. β-Actin served as an internal control. (e) Measurement of mitochondrial membrane depolarization. Data are mean ± SEM from 20 regions of interest (ROI). (f) Western analysis of cytochrome *c* discharge into medium (sup) by HeLa cell mitochondria (pellet) treated with the indicated drugs. (g) Quantitation of drug accumulation in brain mitochondria treated with the indicated drugs compared with the level in the culture medium. Data are mean ± SEM of duplicate samples from two independent experiments.

Imaging of Mitochondrial Membrane Potential. HeLa cells were seeded on a Lab Tek II slide chamber at 40%−80% confluence in DMEM (Lonza) supplemented with 10% FBS and 1% penicillin/streptomycin at 37 °C and 5% CO_2. The cells were labeled with 200 nM TMRM, incubated with 10 μM FCCP, gamitrinib, 17-AAG, DMAG, BIIB-021, PU-H71, AUY922, or DMSO (control) for 30 min, and analyzed using an FV1000 laser confocal scanning microscope (Olympus).

Statistical Analysis. Statistical analyses were performed using the software program Prism 5.0 (GraphPad). In an unpaired *t* test, $p < 0.05$ was considered significant.

RESULTS

TRAP1, Rather than Hsp90, is the Predominant Chaperone in Cancer Cell Mitochondria. To determine the amounts of Hsp90 and TRAP1 in mitochondria of cancer cells, we fractionated several cancer cell types, isolated the mitochondria, and analyzed mitochondrial protein content by quantitative Western blotting. TRAP1 was present at an approximately 10-fold higher level than Hsp90, with 2−3 ng Hsp90 and 18−28 ng TRAP1 in 10 μg mitochondrial protein extract (Figure 1a,b). Next, intrinsic ATPase activity was measured with purified recombinant proteins, and TRAP1 showed an approximately 32-fold higher activity than Hsp90 regarding kinetic parameters (Figure 1c, Table 1), which is consistent with previous reports.[24,29] Mitochondrial Hsp90s have been reported to regulate unfolded protein responses (UPRs) in the endoplasmic reticulum (ER).[18,22,30] We found induction of ER UPRs (elevation of C/EBP homologous protein [CHOP] and increased phosphorylation of eukaryotic translation initiation factor [eIF]2α) after siRNA-mediated TRAP1 knockdown in cells, meaning that specific inactivation of TRAP1 alone by siRNA was enough to induce ER UPRs (Figure 1d). Considering the lack of known cochaperones for proper functioning of Hsp90 in the mitochondria,[31,32] the data strongly argue that in mitochondria of cancer cells, TRAP1 predominates over Hsp90 for triggering the organelle-specific UPRs.

Table 1. Kinetic Parameters of Hsp90 and TRAP1

	Hsp90	TRAP1
K_m (μM)	573.31 ± 91.66	39.69 ± 1.97
k_{cat} (sec^{-1})	1.13 (±0.17) × 10^{-2}	2.52 (±0.01) × 10^{-2}
k_{cat}/K_m (μM^{-1} sec^{-1})	1.98 (±0.12) × 10^{-5}	63.67 (±3.12) × 10^{-5}

DOI: 10.1021/ja511893n
J. Am. Chem. Soc. 2015, 137, 4358−4367

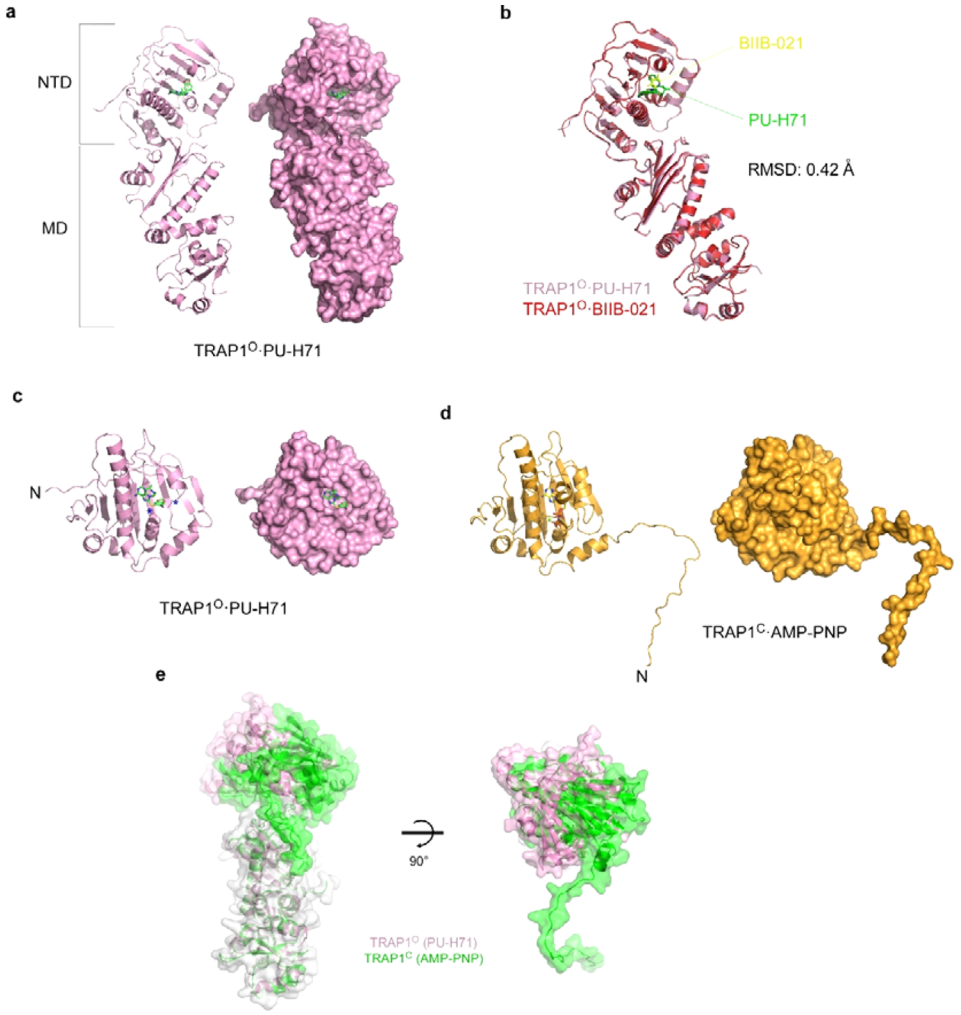

Figure 2. Crystal structures of TRAP1. (a) Overall structure of TRAP1^{O}–PU-H71 complex. Ribbon diagram (left) and surface representation (right) of the open conformation of hTRAP1-NM (TRAP1^{O}, magenta) complexed with PU-H71 (green) in the same orientation. NTD, N-terminal domain; MD, middle domain. (b) Structural comparison of TRAP1^{O}–PU-H71 (magenta) and TRAP1^{O}–BIIB-021 (red). The backbone atoms of hTRAP1-NM in the complexes are superimposed with a root-mean-square deviation (RMSD) of 0.42 Å. (c) Ribbon diagram (left) and surface contour image (right) of NTD structure of TRAP1^{O}–PU-H71. hTRAP1-NM, magenta; PU-H71, green. (d) Ribbon diagram (left) and surface representation (right) of NTD of TRAP1^{C}–AMP-PNP in the same orientation as TRAP1^{O}–PU-H71 in (c). For simplicity, only one protomer in the dimeric structure is depicted. hTRAP1-NM, orange; AMP-PNP, yellow; oxygen, red; phosphorus, orange; and nitrogen, blue; magnesium, green. (e) Comparison of the overall conformations of TRAP1^{O} and TRAP1^{C} in surface contour images. The MD (corresponding to residues 298–553 and depicted as transparent white) of TRAP1^{O} (magenta) and one TRAP1^{C} protomer (green) were superimposed with an RMSD of 1.36 Å, and conformation of the NTDs were compared (left); 90° rotation around a horizontal axis (right).

There has been controversy over whether Hsp90 inhibitors can penetrate mitochondrial membranes.[12,15] The mitochondria-targeted Hsp90 inhibitor gamitrinib triggered loss of fluorescence signal from the mitochondrial membrane potential-sensitive dye tetramethylrhodamine (TMRM) in HeLa cells (Figure 1e and Supporting Information, Figure S7) and discharge of intermembrane space protein cytochrome c from isolated mitochondria (Figure 1f), which is indicative of mitochondrial membrane depolarization and outer membrane permeabilization, as reported previously.[15] However, the Hsp90 inhibitors 17-AAG, DMAG, BIIB-021, PU-H71, and AUY922 did not achieve the same results (Figure 1e,f and Supporting Information, Figure S7). The concentration of the drugs that accumulated in mitochondria was directly measured with liquid chromatography/triple quadrupole mass spectrometry.[33] Greater than 90% of PU-H71, DMAG, BIIB-021, and AUY922 was found in the medium (outside mitochondria), whereas gamitrinib accumulated to an approximately 100-fold higher level in mitochondria than in the medium (Figure 1g). Thus, the data suggest that drug accumulation in the mitochondrial compartment should be an important consideration when designing effective inhibitors to target proteins in this organelle. Conjugation of organelle-specific delivery systems to inhibitors can resolve this issue, as previously reported.[15,16]

Crystal Structures of TRAP1–Hsp90 Inhibitor Complex. To better understand the mechanism of molecular recognition of Hsp90 inhibitors by TRAP1, the structures of TRAP1–inhibitor complexes were determined. Initially, we obtained crystals of the full-length mitochondrial form of human TRAP1 (amino acid residues 60–704), but they were of low crystallographic quality. Instead, TRAP1 lacking the C terminal domain (CTD) (residues 60–561), designated as hTRAP1-NM, was crystallized with purine-scaffold Hsp90 inhibitors (PU-H71 and BIIB-021) or an ATP analogue (AMP-PNP), and their structures were refined at a resolution of 2.7 Å, 3.1 Å, and 3.3 Å, respectively (Supporting Information, Table S1).[24] Both

DOI: 10.1021/ja511893n
J. Am. Chem. Soc. 2015, 137, 4358–4367

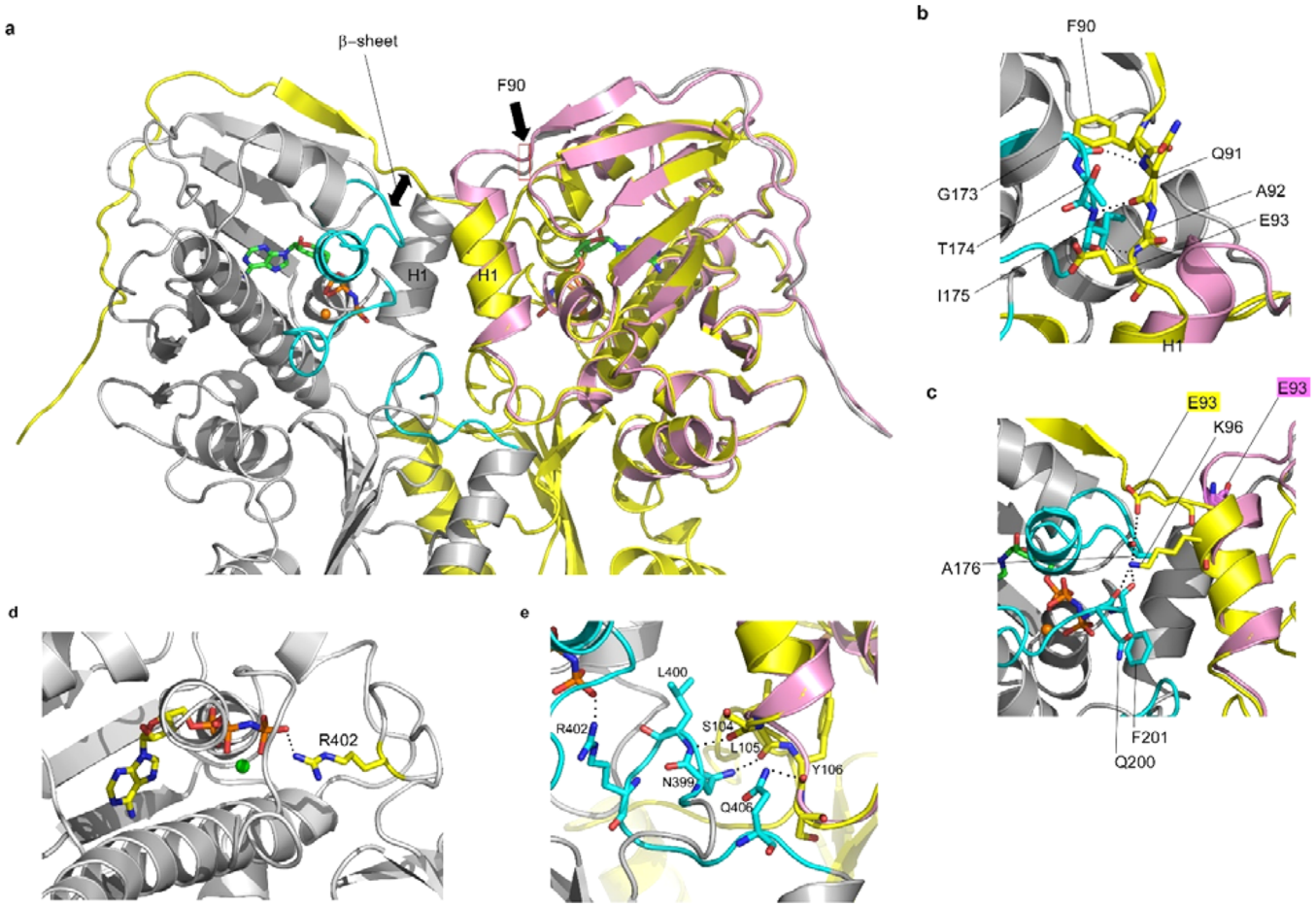

Figure 3. Comparison of TRAP1 structures. (a) Overlay of structures of hTRAP1-NM complexed with PU-H71 and AMP-PNP. hTRAP1-NM−PU-H71 and hTRAP1-NM−AMP-PNP are shown in magenta and gray/yellow, respectively. The middle domain of the TRAP1^{O}−PU-H71 complex has been deleted for clarity. Stabilized residues corresponding to the active site lid and ATP sensor loop upon AMP-PNP binding are shown in cyan. The first α-helix is labeled H1. The location of F90 is indicated with a single-headed arrow. The short β-sheet structure in hTRAP1-NM−AMP-PNP is indicated by a double-headed arrow. (b) Tripeptide β-sheet-like structure in TRAP1^{C}−AMP-PNP. Stabilized ATP lid (cyan) from one protomer (gray) interacts with N-terminus of helix H1 from the other protomer (yellow). Amino acid residues forming tripeptide β-sheet are indicated. Helix H1 is unwound to form a dimer in hTRAP1-NM−AMP-PNP (yellow), which is different from hTRAP1-NM−PU-H71 (magenta). Oxygen atoms, red; nitrogen atoms, blue. Black dotted lines indicate intermolecular H-bonds between two protomers of the hTRAP1-NM dimer. (c) Dimer interface between helix H1 and stabilized lid structure. Side chains E93 and K96 form H-bonds with A176, Q200, and F201 in the main chain in the stabilized active site lid. (d) Interaction of ATP γ-phosphate and R402 is indicated by dotted line. The green sphere indicates a magnesium atom. (e) Ribbon diagram shows residues involved in interaction between the ATP-stabilized sensor loop (cyan) and C-terminus of H1 from the opposite protomer (yellow).

hTRAP1-NM−PU-H71 and hTRAP1-NM−BIIB-021 had monomeric architecture (Figure 2a,b), primarily due to deletion of the dimerization domain CTD,[34] and significant structural differences between the two were not observed, with a root-mean-square deviation (RMSD) of 0.42 Å for all Cα atoms (Figure 2b). In contrast, AMP-PNP-bound hTRAP1-NM was a dimer (Supporting Information, Figure S1a), and had very similar overall conformation to full-length zebrafish TRAP1 (zTRAP1) complexed with AMP-PNP[34] (RMSD = 1.23 Å, Figure S1b), but lacked the dramatic protomer−dimer asymmetry observed in zTRAP1 (Figure S1c). Our hTRAP1-NM−AMP-PNP structure, however, crystallized as a dimer within the asymmetric unit even in the absence of the CTD. The dimeric form of hTRAP1-NM showed extensive *trans* protomer interaction through exchange of the "strap"-like N-terminal sequences, which further stabilizes the N-terminal domain (NTD) dimer, a feature similar to that seen in zTRAP1[34] (Figure S1a,b); in contrast, the strap sequence of monomeric hTRAP1-NM wraps around itself, that is, through *cis* interaction (Figure 2a,b). The active site lid structure (residues 172−201) of the ATP-binding pocket is disordered in the inhibitor-bound hTRAP1-NM NTD (Figure 2c), thereby largely exposing the pocket to the solvent (Figure S2a). The structure showing this open conformation is designated TRAP1^{O} here. However, in complexes of hTRAP1-NM bound to ATP analogue AMP-PNP (designated TRAP1^{C}, indicating the closed conformation), the lid structure is well ordered and closes the ATP-binding pocket to sequester the bound ligand from the solvent (Figure 2d), which is similar to the zebrafish TRAP1[34] (Figure S2b). Comparison of overall NTD and MD structures of TRAP1^{O} and TRAP1^{C} showed gross conformational differences at the hinge region between the domains (Figure 2e, S3a−c), consistent with the previous report from the Agard group.[34]

Dimer Interface Stabilization and Conformational Changes by AMP−PNP Binding. Structural comparison showed three major differences causing global conformational changes between the open and closed conformations of hTRAP1-NM. As shown in Figure 3a, these differences were in

DOI: 10.1021/ja511893n
J. Am. Chem. Soc. 2015, 137, 4358−4367

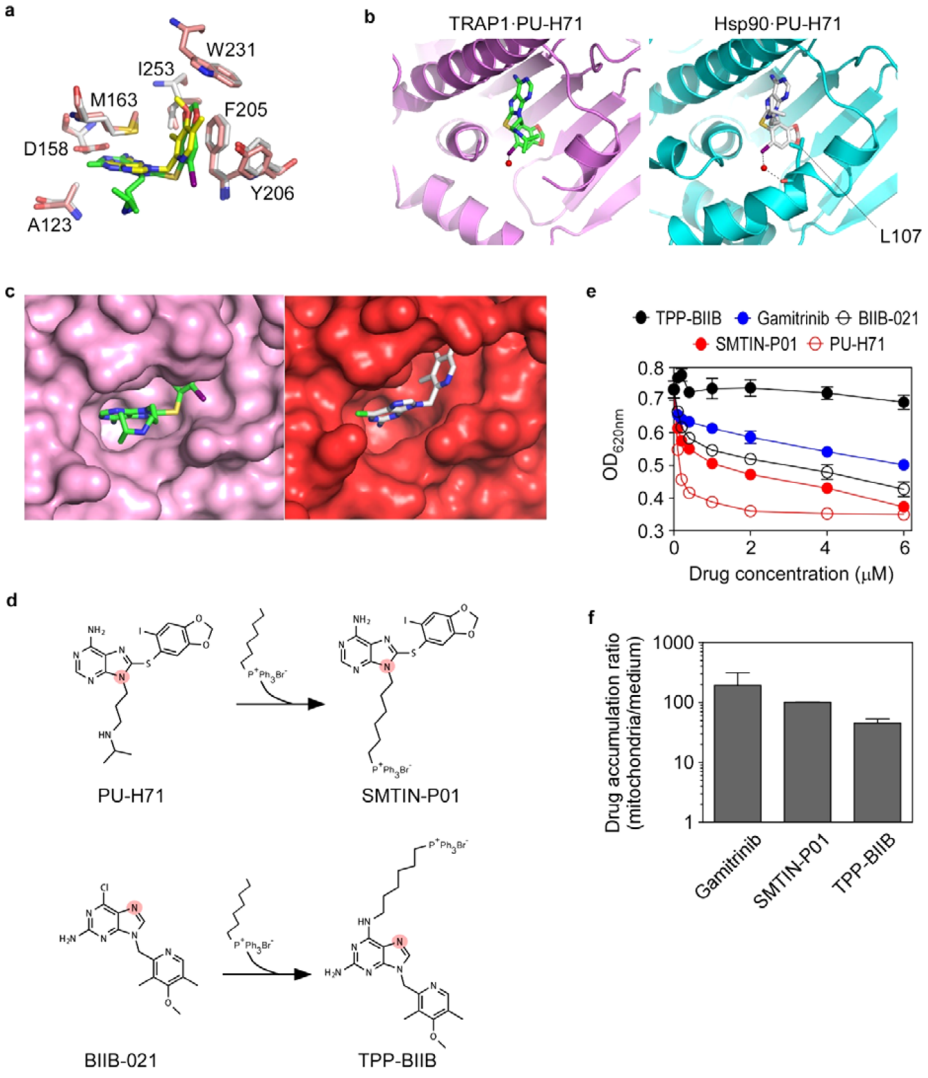

Figure 4. Structure-based modification of Hsp90 inhibitors. (a) Conserved amino acid residues in the ATP pocket. Structures of PU-H71-bound Hsp90 (gray) and hTRAP1-NM (magenta) are overlaid. Numbering is for TRAP1. (b) Comparison of the structures of hTRAP1-NM (left) and Hsp90 (right) complexed with PU-H71. (c) hTRAP1-NM ATP pocket bound to PU-H71 (left) and BIIB-021 (right). (d) TPP conjugates of PU-H71 and BIIB-021. The TPP-hexyl linker was conjugated to PU-H71 and BIIB-021 to produce SMTIN-P01 and TPP-BIIB, respectively. The red circles indicate the most solvent exposed atoms. (e) Inhibition of TRAP1 ATPase activity by the mitochondria-targeted and nontargeted inhibitors. The data are mean ± SEM from two independent triplicate experiments. (f) Quantitation of drug accumulation in brain mitochondria treated with the indicated drugs compared with the level in culture medium. Data are mean ± SEM from duplicated two independent experiments.

(1) the hinge region of the N-terminal strap, (2) the active site lid structure, and (3) the ATP sensor (R402) loop stabilization. When the *cis* interactions changed to *trans* interactions upon ATP binding, there was no change in the overall strap configuration from the N-terminus to F90. However, an H-bonding network was newly established between the main chains of the strap hinge at residues Q91, A92, and E93 on one protomer and the stabilized active site lid segment at residues G173, T174, and I175 on the other protomer, which resulted in formation of a short parallel β-sheet–like structure in TRAP1^{C} (Figure 3b). The main chain from the lid segment (A176, Q200, and F201) also establishes an interprotomer H-bonding network with side chains of the strap hinge region amino acid residues E93 and K96 in TRAP1^{C} (Figure 3c). The interprotomer interaction between the strap hinge and the active site lid shown in Figure 3a–c accompanies stabilization (Supporting Information, Figure S4a), half-turn unwinding, and 13° tilting of the first α-helix (helix H1) (Figure S4b). An absolutely conserved Arg residue from MD (R380 for Hsp90 and R402 for TRAP1), establishes an ionic interaction with the γ-phosphate of ATP and has been suggested to be an ATP sensor that stabilizes the closed conformation.[35] The loop structure (residues 398–407) containing the sensor amino acid residue R402 is disordered in the TRAP1^{O} structure (Supporting Information, Figure S5a) but the loop structures are stabilized in both human and zebrafish TRAP1^{C} (Figure S5b,c). Ionic interaction between R402 and γ-phosphate was clearly seen in TRAP1^{C} (Figure 3d), which stabilized the ATP sensor loop structure (Figure 3e, cyan). The stabilized ATP sensor loop establishes interprotomer H-bonding networks with the C-terminus of the main H1 helix chain (S104, L105, and Y106), which might further contribute to the stabilization of helix H1 in TRAP1^{C}. Analytical ultracentrifugation showed that, in the presence of AMP-PNP, molecular weight in an amount equivalent to that of the hTRAP1-NM was shifted to the dimer, whereas dimerization was fully inhibited by R402A mutation (Supporting Information, Figure S6a) without

DOI: 10.1021/ja511893n
J. Am. Chem. Soc. 2015, 137, 4358–4367

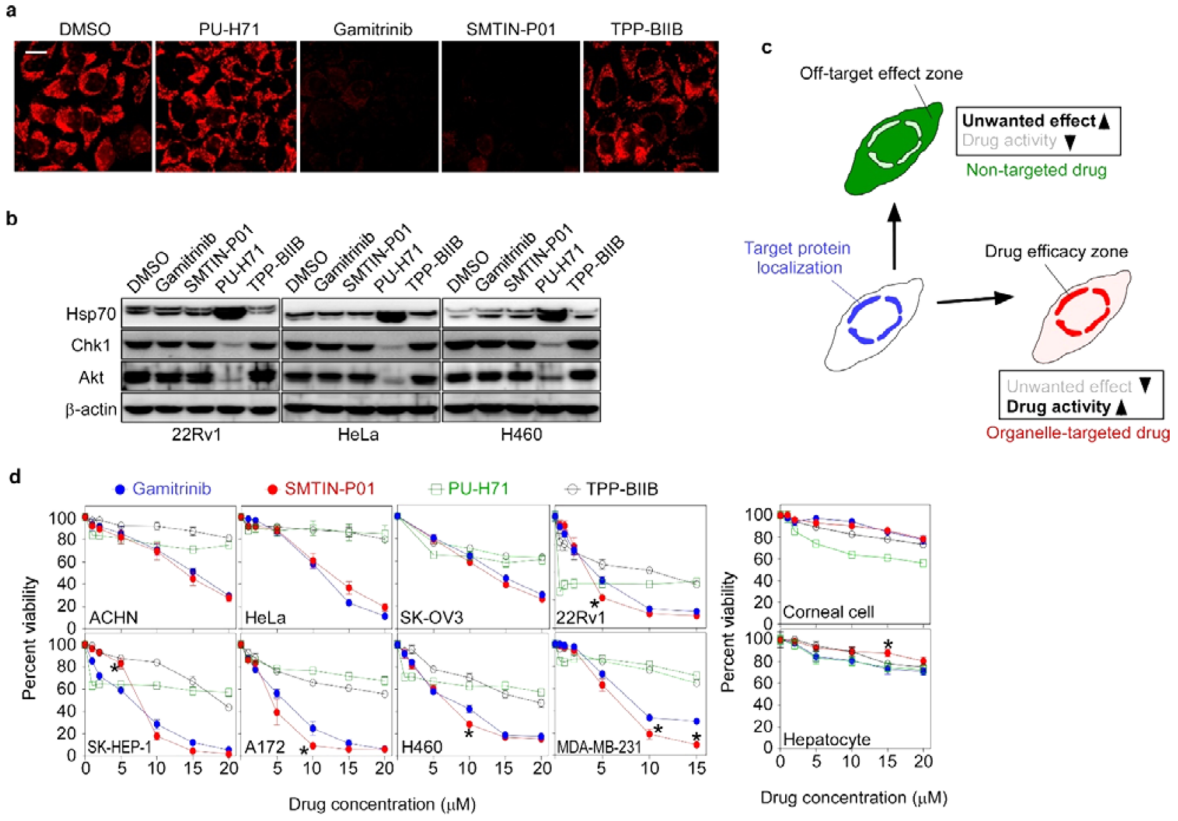

Figure 5. Improved cytotoxicity of SMTIN-P01. (a) Fluorescence analysis of mitochondrial membrane potential in tetramethylrhodamine (TMRM)-loaded HeLa cells treated with the indicated drugs. Scale bar, 20 μm. (b) Western analysis of Hsp70 upregulation and depletion of Hsp90 clients Chk1 and Akt in indicated cell types, treated with the indicated drugs (2 μM) for 24 h. (c) Modulation of organelle-resident protein using organelle-targeted and nontargeted drugs. The organelle (here, mitochondrion) is outlined, and the suborganellar target protein is shown in blue. Nontargeted drugs will accumulate largely outside and, to some extent, inside (green) the organelle, whereas the targeted drug will accumulate largely at the site of target localization (red), which might improve drug activity and alleviate unwanted off-target effects. (d) Viability of cancer cells derived from kidney (ACHN), cervix (HeLa), ovary (SK-OV3), prostate (22Rv1), liver (SK-HEP-1), brain (A172), lung (H460), and breast (MDA-MB-231) (left) and normal human corneal cells and mouse primary hepatocytes (right) after treatment with the indicated drugs. Data are mean ± SEM of triplicate samples from two independent experiments. *$p < 0.05$ for SMTIN-P01 compared with gamitrinib.

loss of ATP binding (Figure S6b), suggesting the crucial function of the conserved Arg residue in NTD dimerization and conformational change in hTRAP1-NM.

Modification of Purine-Scaffold Hsp90 Inhibitors: Development of SMTIN-P01. To generate TRAP1-specific inhibitors, we compared the ATPase pocket structures of Hsp90 and TRAP1 complexed with Hsp90 inhibitors. ATP-binding sites of TRAP1 and Hsp90 showed very similar arrangements of crucial residues and structural water molecules interacting with the inhibitors PU-H71 and BIIB-021 (Figure 4a).[36] Hsp90 D102 was replaced with E167 in TRAP1, which results in loss of one water molecule in TRAP1 due to increased bulkiness (Supporting Information, Figure S8) and is not expected to significantly affect the protein-inhibitor interaction. However, hydrophobic interaction and water-mediated H-bonding of L107 in Hsp90 (corresponding to L172 in TRAP1) with PU-H71 is not observed in the TRAP1 structure due to the disordered ATP lid (Figure 4b). Slightly reduced binding affinity of PU-H71 for TRAP1 compared with Hsp90[37] may originate, at least in part, from the lack of these molecular interactions. Thus, in order to generate high-affinity inhibitors of TRAP1, additional interactions that can stabilize the flexible active site lid structure, including the hydrophobic L172 residue, may be required. We can conclude, however, that the rational development of TRAP1-selective inhibitors is not readily doable based on the highly conserved active site residues and almost superimposable nucleotide-binding site structures among Hsp90 paralogues (Figure 4a);[38] therefore, alternatively, we decided to design subcellular compartment-specific inhibitors through TPP conjugation to achieve mitochondrial TRAP1 selectivity. After structural comparison, we identified possible conjugation sites for representative Hsp90 inhibitors (Supporting Information, Figure S9). We decided to synthesize TPP-conjugated PU-H71 on the basis of robust biological data, synthetic tractability, and chemical synthesis feasibility of this inhibitor.[36,37,39] In the case of PU-H71, the N9 position of the purine ring is oriented toward the solvent (Figure 4c,d). The solvent-exposed N9 alkane of the PU-H71 purine ring was substituted with alkylated TPP to make an active inhibitor, designated as SMTIN-P01, whereas the poorly exposed chlorine of BIIB-021 was substituted with alkylated TPP to make an inactive control compound. The actual binding affinity of SMTIN-P01 was slightly lower than that of PU-H71 and higher than gamitrinib, whereas TPP-BIIB was almost inactive based on the inhibition of TRAP1 ATPase activity (Figure 4e). However, accumulation of the TPP conjugates SMTIN-P01, TPP-BIIB, and gamitrinib in mitochondria was dramatically enhanced compared to their respective parental compounds (Figures 1g and 4f). TPP-driven drug delivery was significantly affected by the chemical properties of the conjugated Hsp90 inhibitors, considering that the accumu-

DOI: 10.1021/ja511893n
J. Am. Chem. Soc. 2015, 137, 4358−4367

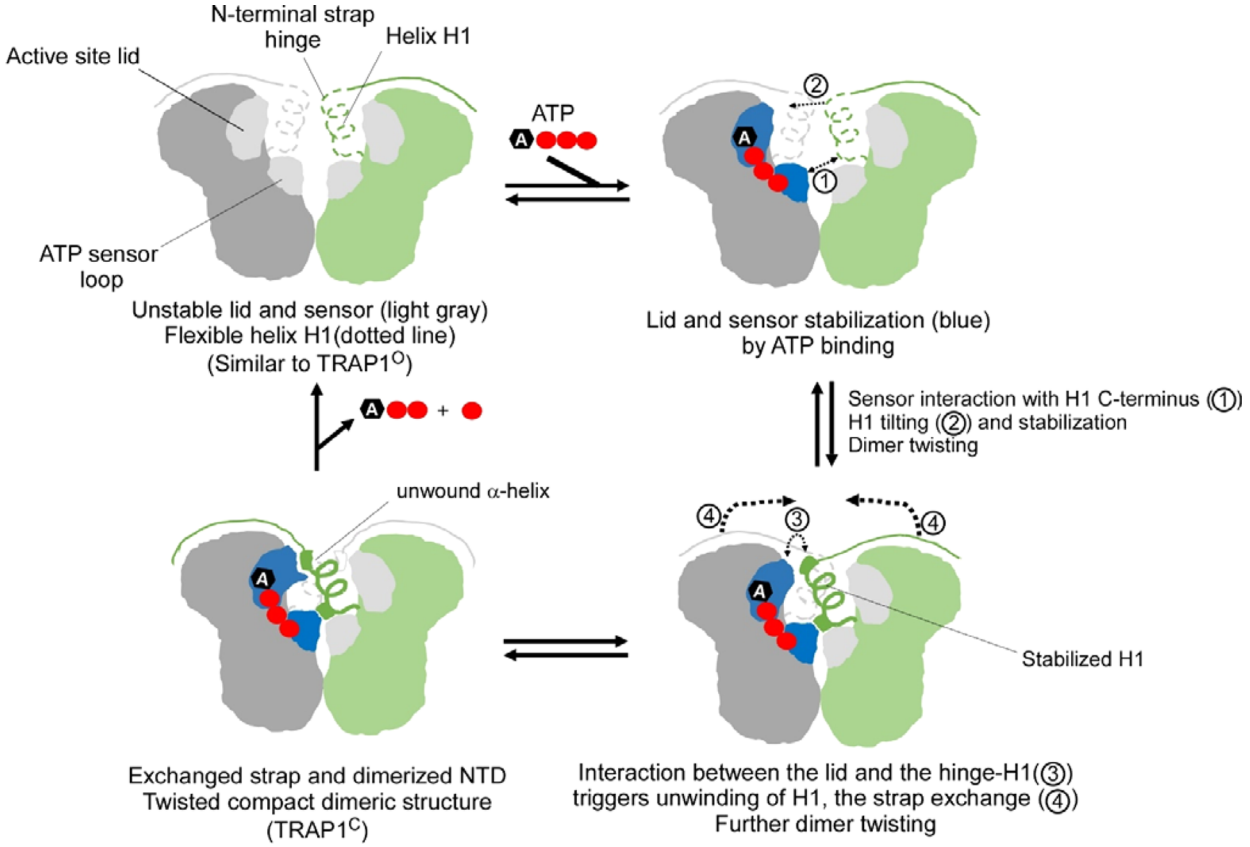

Figure 6. Proposed model for TRAP1 N-terminal domain dimerization and ATPase cycle. The apo form of the TRAP1 dimer (top left), similar to the structure of TRAP1^{O}, has a disordered active site lid and ATP sensor loop and a flexible helix H1. Upon ATP binding (top right), the active site lid and the ATP sensor loop become stabilized (blue), permitting establishment of interprotomer interaction between the sensor and C-terminus of helix H1 (1). This potentially moves the H1 of one protomer into close proximity to the active site lid of the other protomer by tilting the helix (2). Now, the stabilized active site lid can bind to the strap hinge and N-terminus of helix H1 from the other protomer (3), which triggers unwinding of N-terminal H1 and, finally, strap exchange (4) (bottom right). In parallel with the helix H1 conformational changes, TRAP1 adopts the tightly packed, twisted TRAP1^{C} conformation, ready to hydrolyze ATP (bottom left).

lation of gamitrinib in the mitochondria was approximately 2-fold and 4-fold greater than that of SMTIN-P01 and TPP-BIIB, respectively (Figure 4f). To investigate whether SMTIN-P01 affects the overall conformation of TRAP1, we crystallized an hTRAP1-NM−SMTIN-P01 complex. The hTRAP1-NM−SMTIN-P01 crystals were grown under the same conditions as hTRAP1-NM−PU-H71 crystals, and the structure was refined at a resolution of 2.9 Å. The TPP moiety was disordered, and we were unable to model the structure (Supporting Information, Figure S10a). No significant difference was observed between hTRAP1-NM−SMTIN-P01 and hTRAP1-NM−PU-H71 (Figure S10b, RMSD = 0.46 Å), suggesting that conjugation of TPP to PU-H71 did not affect the binding mode of PU-H71 to TRAP1.

Cytotoxic Activity of SMTIN-P01. SMTIN-P01, similar to gamitrinib, was able to induce mitochondrial membrane depolarization in HeLa cells, whereas the nontargeted Hsp90 inhibitor, PU-H71, and the targeted, inactive Hsp90 inhibitor, TPP-BIIB, did not affect mitochondrial membrane potential (Figure 5a). PU-H71 treatment induced the signature responses to Hsp90 inhibition,[3,40] including depletion of the Hsp90 client proteins Chk1 and Akt and upregulation of Hsp70, whereas treatment with SMTIN-P01, gamitrinib, or TPP-BIIB failed to induce these responses (Figure 5b). These data indicate that mitochondria-specific delivery can change pan-Hsp90 inhibitors into specific inhibitors of the mitochondrial paralogue (Figure 5c). Considering that application of certain drugs is limited due to nonspecific inactivation of several homologous proteins localized in different subcellular compartments, the concept described in Figure 5c can be broadly exploited to specifically inactivate mitochondrial target proteins and to improve drug activity. SMTIN-P01 showed stronger cytotoxicity against all the cancer cells than the parental Hsp90 inhibitor PU-H71 and slightly improved cytotoxicity over gamitrinib in some cancer cells, including 22Rv1, A172, H460, and MDA-MB-231 (Figure 5d, left). The weaker binding affinity of geldanamycin (in gamitrinib) than the PU-H71 moiety in TPP conjugates[37] (Figure 4e) seems to be compensated by better mitochondrial accumulation (Figure 4f), which further suggests the importance of drug accumulation in the mitochondria for activity of organelle-specific inhibitors. Normal corneal cells and hepatocytes were marginally affected by all of the compounds tested, but SMTIN-P01 was slightly less cytotoxic to hepatocytes than gamitrinib and PU-H71 (Figure 5d, right). The data indicate that mitochondrial targeting of the Hsp90 inhibitor can generate a potent cancer cell-specific cytotoxic agent with a mechanism of action that is quite different from that of the nontargeted parental compound.

■ DISCUSSION

Hsp90 has been reported to be induced under cellular stress conditions;[41] therefore, mitochondrial levels of Hsp90 might

DOI: 10.1021/ja511893n
J. Am. Chem. Soc. 2015, 137, 4358−4367

possibly be elevated to supplement TRAP1 functions under conditions of increased demand for chaperone functions in the mitochondria.[42] Therefore, we cannot completely exclude the possibility of unappreciated functions of mitochondrial Hsp90 under certain conditions of cellular stress. Our data, however, strongly argue that TRAP1, rather than Hsp90, is the predominant chaperone in cancer cell mitochondria and plays a key role in suppressing UPR induction. This hypothesis is supported by previous data showing the small amount of Hsp90 in mitochondria with intrinsic low ATPase activity and the lack of known cochaperones for full Hsp90 chaperone activity.[31,32]

Many mitochondrial proteins involved in cell death and metabolic pathways have emerged as drug targets for a variety of human diseases.[43,44] Here, we showed that many Hsp90 inhibitor molecules do not accumulate efficiently inside mitochondria. This suggests that mitochondrial accumulation should be considered an important property when developing molecules to target mitochondrial proteins. In addition, organelle-specific delivery of drugs could minimize off-target effects by avoiding drug accumulation in nontarget subcellular compartments, while maximizing drug efficacy by elevating the local concentration of the drug at the site of target protein localization. Considering that mitochondrial delivery of Hsp90 inhibitors altered the mode of drug action, manipulation of subcellular location of certain inhibitors may show previously unidentified regulation of cell physiology, depending on the function of compartmentalized target proteins. Therefore, the activities of many inhibitors targeting mitochondrial proteins may require reevaluation based on their mitochondrial accumulation efficiency, and may require redesign as mitochondria-targeted to improve desirable drug activities while minimizing unwanted side effects. It has been suggested that redirecting drugs to mitochondria by conjugation to TPP results in greater accumulation of the drugs in tumor than in normal tissues *in vivo*,[45,46] probably due to elevated mitochondrial membrane potentials in cancer cells.[47] Therefore, mitochondrial delivery of the drug will further enhance cancer-specific activity.

A comparison of crystal structures of hTRAP1-NM complexed with PU-H71 and AMP-PNP might explain the nature of conformational change in TRAP1, which is important for understanding the mechanism of ATP-driven chaperone functions.[48,49] It has been reported that Hsp90 inhibitors can mimic the ADP-bound conformation of Hsp90 in terms of shape complementarity and molecular interaction networks[50,51] and, in our study, the inhibitor-bound hTRAP1-NM structure $TRAP1^{O}$ showed a monomeric and open conformation, a catalytically incompetent state.[52] These data strongly support the idea that $TRAP1^{O}$ can mimic or reflect the structure of the ADP-bound or apo forms of TRAP1, which lack the ionic interaction between R402 and ATP γ-phosphate. Considering that ligand binding largely stabilizes Hsp90 protein family structures,[53] apo-TRAP1 is likely to have a more flexible conformation than $TRAP1^{O}$.

On the basis of our structural analysis, we propose the molecular mechanism of the ATPase cycle of TRAP1 as shown in Figure 6. Non-ligand-bound TRAP1 has largely relaxed structures. The active site lid, ATP sensor loop, and helix H1 are all flexible. Upon ATP binding, the lid and ATP sensor loop become rigid, which attracts the helix H1 of the other protomer and subsequently induces tilting of the H1 helix. Further interaction of the H1 N-terminus of one protomer with the lid of the other protomer unwinds the H1 α-helix by a half turn and triggers exchange of the N-terminal straps to establish extensive interprotomer interaction through the N-terminal strap sequences, which finally results in full dimerization of the TRAP1 NTD and hinge point rotation at domain interfaces to achieve a global conformational change to a compact twisted dimer structure. Therefore, the conformation of the helix H1, located at the dimer interface, is critically modified upon ATP binding, which plays a crucial role in leveraging the global conformational change of the TRAP1 structure.

■ CONCLUSIONS

In this study, we identified TRAP1 as the mitochondrial target protein for cancer drug development and also addressed the limitation of current Hsp90 inhibitors for TRAP1 inactivation, primarily due to the inefficient accumulation of the drugs in the mitochondria. To overcome the limited effects of these drugs on mitochondrial TRAP1 and increase drug anticancer activity, we designed Hsp90 inhibitor conjugates with the mitochondrial delivery moiety TPP after comparison of crystal structures of TRAP1 and Hsp90 complexed with Hsp90 inhibitors. We synthesized the mitochondria-accumulating Hsp90 inhibitor SMTIN-P01, a conjugate of PU-H71 and TPP, and showed mitochondrial Hsp90 paralogue (TRAP1)-specific activity of the compound. Therefore, Hsp90 inhibitors can be rationally designed for delivery into the mitochondria for development of mitochondrial Hsp90 paralogue-specific inhibitors. The concept of the organelle-specific drugs can be exploited, not only for Hsp90 inhibitors, but also for other therapeutics targeting mitochondrial proteins to improve drug activity, minimize side effects, and often alter the mode of drug action. In addition, we showed crystal structures of both the open and closed TRAP1 conformations, and can, therefore, suggest molecular mechanisms of conformational change during the TRAP1 ATPase cycle, which will also aid in understanding the general mechanisms of the Hsp90 chaperone function.

■ ASSOCIATED CONTENT

Supporting Information

Synthetic details of SMTIN-01 and TPP-BIIB, mitochondrial membrane depolarization by various chemicals, structural analysis of TRAP1-AMP-PNP complex, structure of NTD of ligand bound TRAP1, structural comparison between $TRAP1^{O}$ and $TRAP1^{C}$, the stability and conformation of helix H1 in $TRAP1^{O}$ and $TRAP1^{C}$, the middle domain in $TRAP1^{O}$ and $TRAP1^{C}$, TRAP1 NTD dimerization, structural comparison between TRAP1−PU-H71 and Hsp90−PU-H71, proposed TPP-conjugates for Hsp90 inhibitors, structural comparison between TRAP1−PU-H71 and TRAP1−SMTIN-P01. Atomic coordinates and structure factors for the hTRAP1-NM−PU-H71, hTRAP1-NM−BIIB-021, hTRAP1-NM−SMTIN-P01 and hTrap1-NM-AMP-PNP structures have been deposited in the Protein Data Bank under PDB code 4Z1F, 4Z1G, 4Z1H and 4Z1I, respectively. This material is available free of charge via the Internet at http://pubs.acs.org.

■ AUTHOR INFORMATION

Corresponding Authors

changwook@unist.ac.kr
jhryu@unist.ac.kr
kangbh@unist.ac.kr

Author Contributions

#C.L. and H.-K.P. contributed equally to this work.

Notes

The authors declare no competing financial interest.

DOI: 10.1021/ja511893n
J. Am. Chem. Soc. 2015, 137, 4358−4367

■ ACKNOWLEDGMENTS

We thank the staff at PAL beamline 5C for use of, and assistance with, synchrotron facilities. H.K.P. was supported by a National Junior Research Fellowship from the National Research Foundation of Korea (NRF-2011-0011833). This work was supported by the Science Research Center Programs (2010-0028684) and the Basic Science Research Program (2010-0003586, 201135BC00024) through the National Research Foundation of Korea, the Korea Health Technology R&D Project through the Korea Health Industry Development Institute (KHIDI) funded by the Ministry of Health & Welfare of Korea (HI12C1744), and Korea Drug Development Fund (KDDF-201312-06).

■ REFERENCES

(1) Taipale, M.; Jarosz, D. F.; Lindquist, S. *Nat. Rev. Mol. Cell Biol.* **2010**, *11*, 515.
(2) Jhaveri, K.; Taldone, T.; Modi, S.; Chiosis, G. *Biochim. Biophys. Acta* **2012**, *1823*, 742.
(3) Trepel, J.; Mollapour, M.; Giaccone, G.; Neckers, L. *Nat. Rev. Cancer* **2010**, *10*, 537.
(4) Whitesell, L.; Lin, N. U. *Biochim. Biophys. Acta* **2012**, *1823*, 756.
(5) Kang, B. H.; Plescia, J.; Dohi, T.; Rosa, J.; Doxsey, S. J.; Altieri, D. C. *Cell* **2007**, *131*, 257.
(6) Agorreta, J.; Hu, J.; Liu, D.; Delia, D.; Turley, H.; Ferguson, D. J.; Iborra, F.; Pajares, M. J.; Larrayoz, M.; Zudaire, I.; Pio, R.; Montuenga, L. M.; Harris, A. L.; Gatter, K.; Pezzella, F. *Mol. Cancer Res.* **2014**, *12*, 660−669.
(7) Caino, M. C.; Chae, Y. C.; Vaira, V.; Ferrero, S.; Nosotti, M.; Martin, N. M.; Weeraratna, A.; O'Connell, M.; Jernigan, D.; Fatatis, A.; Languino, L. R.; Bosari, S.; Altieri, D. C. *J. Clin. Invest.* **2013**, *123*, 2907.
(8) Chae, Y. C.; Angelin, A.; Lisanti, S.; Kossenkov, A. V.; Speicher, K. D.; Wang, H.; Powers, J. F.; Tischler, A. S.; Pacak, K.; Fliedner, S.; Michalek, R. D.; Karoly, E. D.; Wallace, D. C.; Languino, L. R.; Speicher, D. W.; Altieri, D. C. *Nat. Commun.* **2013**, *4*, 2139.
(9) Sciacovelli, M.; Guzzo, G.; Morello, V.; Frezza, C.; Zheng, L.; Nannini, N.; Calabrese, F.; Laudiero, G.; Esposito, F.; Landriscina, M.; Defilippi, P.; Bernardi, P.; Rasola, A. *Cell Metab.* **2013**, *17*, 988.
(10) Yoshida, S.; Tsutsumi, S.; Muhlebach, G.; Sourbier, C.; Lee, M. J.; Lee, S.; Vartholomaiou, E.; Tatokoro, M.; Beebe, K.; Miyajima, N.; Mohney, R. P.; Chen, Y.; Hasumi, H.; Xu, W.; Fukushima, H.; Nakamura, K.; Koga, F.; Kihara, K.; Trepel, J.; Picard, D.; Neckers, L. *Proc. Natl. Acad. Sci. U.S.A.* **2013**, *110*, E1604.
(11) Chae, Y. C.; Caino, M. C.; Lisanti, S.; Ghosh, J. C.; Dohi, T.; Danial, N. N.; Villanueva, J.; Ferrero, S.; Vaira, V.; Santambrogio, L.; Bosari, S.; Languino, L. R.; Herlyn, M.; Altieri, D. C. *Cancer cell* **2012**, *22*, 331.
(12) Rasola, A.; Neckers, L.; Picard, D. *Trends Cell Biol.* **2014**, *24*, 455−463.
(13) Altieri, D. C. *Oncotarget* **2011**, *2*, 347.
(14) Murphy, M. P.; Smith, R. A. *Annu. Rev. Pharmacol. Toxicol.* **2007**, *47*, 629.
(15) Kang, B. H.; Plescia, J.; Song, H. Y.; Meli, M.; Colombo, G.; Beebe, K.; Scroggins, B.; Neckers, L.; Altieri, D. C. *J. Clin. Invest.* **2009**, *119*, 454.
(16) Kang, B. H. *BMB Rep.* **2012**, *45*, 1.
(17) Hoye, A. T.; Davoren, J. E.; Wipf, P.; Fink, M. P.; Kagan, V. E. *Acc. Chem. Res.* **2008**, *41*, 87.
(18) Siegelin, M. D.; Dohi, T.; Raskett, C. M.; Orlowski, G. M.; Powers, C. M.; Gilbert, C. A.; Ross, A. H.; Plescia, J.; Altieri, D. C. *J. Clin. Invest.* **2011**, *121*, 1349.
(19) Kang, B. H.; Tavecchio, M.; Goel, H. L.; Hsieh, C. C.; Garlick, D. S.; Raskett, C. M.; Lian, J. B.; Stein, G. S.; Languino, L. R.; Altieri, D. C. *Br. J. Cancer* **2011**, *104*, 629.
(20) Kang, B. H.; Siegelin, M. D.; Plescia, J.; Raskett, C. M.; Garlick, D. S.; Dohi, T.; Lian, J. B.; Stein, G. S.; Languino, L. R.; Altieri, D. C. *Clin. Cancer Res.* **2010**, *16*, 4779.
(21) Park, H. K.; Lee, J. E.; Lim, J.; Jo, D. E.; Park, S. A.; Suh, P. G.; Kang, B. H. *BMC Cancer* **2014**, *14*, 431.
(22) Park, H. K.; Lee, J. E.; Lim, J.; Kang, B. H. *Mol. Cancer* **2014**, *13*, 148.
(23) Li, W. C.; Ralphs, K. L.; Tosh, D. *Methods Mol. Biol.* **2010**, *633*, 185.
(24) Jeong, H.; Kang, B. H.; Lee, C. *Acta Crystallogr. F Struct. Biol. Commun.* **2014**, *70*, 1683.
(25) Otwinowski, Z.; Minor, W. *Methods Enzymol.* **1997**, *276*, 307.
(26) Adams, P. D.; Afonine, P. V.; Bunkoczi, G.; Chen, V. B.; Davis, I. W.; Echols, N.; Headd, J. J.; Hung, L. W.; Kapral, G. J.; Grosse-Kunstleve, R. W.; McCoy, A. J.; Moriarty, N. W.; Oeffner, R.; Read, R. J.; Richardson, D. C.; Richardson, J. S.; Terwilliger, T. C.; Zwart, P. H. *Acta Crystallogr. D Biol. Crystallogr.* **2010**, *66*, 213.
(27) Terwilliger, T. C.; Berendzen, J. *Acta Crystallogr. D Biol. Crystallogr.* **1999**, *55*, 849.
(28) McCoy, A. J.; Grosse-Kunstleve, R. W.; Adams, P. D.; Winn, M. D.; Storoni, L. C.; Read, R. J. *J. Appl. Crystallogr.* **2007**, *40*, 658.
(29) Leskovar, A.; Wegele, H.; Werbeck, N. D.; Buchner, J.; Reinstein, J. *J. Biol. Chem.* **2008**, *283*, 11677.
(30) Pellegrino, M. W.; Nargund, A. M.; Haynes, C. M. *Biochim. Biophys. Acta* **2013**, *1833*, 410.
(31) Felts, S. J.; Owen, B. A.; Nguyen, P.; Trepel, J.; Donner, D. B.; Toft, D. O. *J. Biol. Chem.* **2000**, *275*, 3305.
(32) Kamal, A.; Thao, L.; Sensintaffar, J.; Zhang, L.; Boehm, M. F.; Fritz, L. C.; Burrows, F. J. *Nature* **2003**, *425*, 407.
(33) Stone, J. *Methods Mol. Biol.* **2010**, *603*, 203.
(34) Lavery, L. A.; Partridge, J. R.; Ramelot, T. A.; Elnatan, D.; Kennedy, M. A.; Agard, D. A. *Mol. Cell* **2014**, *53*, 330.
(35) Cunningham, C. N.; Southworth, D. R.; Krukenberg, K. A.; Agard, D. A. *Protein Sci.* **2012**, *21*, 1162.
(36) Immormino, R. M.; Kang, Y.; Chiosis, G.; Gewirth, D. T. *J. Med. Chem.* **2006**, *49*, 4953.
(37) Taldone, T.; Patel, P. D.; Patel, M.; Patel, H. J.; Evans, C. E.; Rodina, A.; Ochiana, S.; Shah, S. K.; Uddin, M.; Gewirth, D.; Chiosis, G. *J. Med. Chem.* **2013**, *56*, 6803.
(38) Patel, P. D.; Yan, P.; Seidler, P. M.; Patel, H. J.; Sun, W.; Yang, C.; Que, N. S.; Taldone, T.; Finotti, P.; Stephani, R. A.; Gewirth, D. T.; Chiosis, G. *Nat. Chem. Biol.* **2013**, *9*, 677.
(39) Taldone, T.; Gomes-DaGama, E. M.; Zong, H.; Sen, S.; Alpaugh, M. L.; Zatorska, D.; Alonso-Sabadell, R.; Guzman, M. L.; Chiosis, G. *Bioorg. Med. Chem. Lett.* **2011**, *21*, 5347.
(40) Guo, F.; Rocha, K.; Bali, P.; Pranpat, M.; Fiskus, W.; Boyapalle, S.; Kumaraswamy, S.; Balasis, M.; Greedy, B.; Armitage, E. S.; Lawrence, N.; Bhalla, K. *Cancer Res.* **2005**, *65*, 10536.
(41) Parsell, D. A.; Lindquist, S. *Annu. Rev. Genet.* **1993**, *27*, 437.
(42) Lisanti, S.; Tavecchio, M.; Chae, Y. C.; Liu, Q.; Brice, A. K.; Thakur, M. L.; Languino, L. R.; Altieri, D. C. *Cell Rep.* **2014**, *8*, 671−677.
(43) Fulda, S.; Galluzzi, L.; Kroemer, G. *Nat. Rev. Drug Discovery* **2010**, *9*, 447.
(44) Walters, A. M.; Porter, G. A., Jr.; Brookes, P. S. *Circ. Res.* **2012**, *111*, 1222.
(45) Mourtada, R.; Fonseca, S. B.; Wisnovsky, S. P.; Pereira, M. P.; Wang, X.; Hurren, R.; Parfitt, J.; Larsen, L.; Smith, R. A.; Murphy, M. P.; Schimmer, A. D.; Kelley, S. O. *PloS one* **2013**, *8*, e60253.
(46) Bernal, S. D.; Lampidis, T. J.; Summerhayes, I. C.; Chen, L. B. *Science* **1982**, *218*, 1117.
(47) Chen, L. B. *Annu. Rev. Cell Biol.* **1988**, *4*, 155.
(48) Pearl, L. H.; Prodromou, C. *Annu. Rev. Biochem.* **2006**, *75*, 271.
(49) Richter, K.; Buchner, J. *Cell* **2006**, *127*, 251.
(50) Roe, S. M.; Prodromou, C.; O'Brien, R.; Ladbury, J. E.; Piper, P. W.; Pearl, L. H. *J. Med. Chem.* **1999**, *42*, 260.
(51) Stebbins, C. E.; Russo, A. A.; Schneider, C.; Rosen, N.; Hartl, F. U.; Pavletich, N. P. *Cell* **1997**, *89*, 239.
(52) Hessling, M.; Richter, K.; Buchner, J. *Nat. Struct. Mol. Biol.* **2009**, *16*, 287.
(53) Ban, C.; Junop, M.; Yang, W. *Cell* **1999**, *97*, 85.

DOI: 10.1021/ja511893n
J. Am. Chem. Soc. 2015, 137, 4358−4367